Mechanics of Materials 97 (2016) 184–198

Contents lists available at ScienceDirect

Mechanics of Materials

journal homepage: www.elsevier.com/locate/mechmat

Viscoelastic damping behavior of structural bamboo material and its microstructural origins

Meisam K. Habibi[a,1], Lik-ho Tam[b], Denvid Lau[b], Yang Lu[a,c,*]

[a] Department of Mechanical and Biomedical Engineering, City University of Hong Kong, 83 Tat Chee Avenue, Kowloon, Hong Kong
[b] Department of Architecture and Civil Engineering, City University of Hong Kong, 83 Tat Chee Avenue, Kowloon, Hong Kong
[c] Centre for Advanced Structural Materials (CASM), City University of Hong Kong, 83 Tat Chee Avenue, Kowloon, Hong Kong

ARTICLE INFO

Article history:
Received 28 November 2015
Revised 28 February 2016
Available online 11 March 2016

Keywords:
Bamboo
Biomechanics
Viscoelasticity
Microstructure
Multi-scale mechanical characterization
Molecular dynamics simulation

ABSTRACT

In this study, the intrinsic viscoelastic mechanical behavior of a hierarchical bio-composite, structural bamboo material, was experimentally investigated and correlated with its microstructural constituents and molecular building blocks. The macroscopic viscoelastic responses of bulk bamboo at ambient temperature and dehydrated condition were evaluated through dynamic compression experiments with various loading frequencies, whereas the localized viscoelasticity of bamboo's microstructural phases, viz. fibers and parenchyma cells, were evaluated separately through series of nano-indentation studies. The viscoelastic responses of the bamboo's building blocks were further evaluated at the molecular level, using the computational creep tests via constant force Steered Molecular Dynamics (SMD) simulations. A phenomenological viscoelastic model was then developed to explain the observed microstructure–viscoelastic property relationship. Based on the model and conducted microstructural characterizations, it was believed that the small evolved viscous phases within the parenchyma cells were mainly responsible for the smaller viscoelasticity in bulk bamboo at lower loading frequencies, whereas the exhibited larger viscoelasticity at higher loading frequencies was stemmed out from the concurrent contribution of fibers and parenchyma cells. The findings could be important for understanding the intrinsic viscoelasticity in other biological materials with hierarchical structures, as well as for optimizing the design of bio-inspired composites with favorable structural properties.

1. Introduction

Natural materials have received increasing interests as promising candidates for sustainable structural applications due to their low cost and abundance, in tropical and subtropical regions (especially, in those developing countries). In particular, structural bamboo material (processed, dehydrated bamboo) has recently received great attention as a green housing and construction material and a highly renewable bio-composite for many industrial applications, because of its very fast growth rate, sufficiently low weight and commendable mechanical performance (Scurlock et al., 2000; Chung and Yu, 2002; Gibson, 2012; Dixon and Gibson, 2014). In addition, bamboo's hierarchical biological structure along with its supremacy in mechanical behavior has made bamboo a proficient template for bio-mimicking purposes to design bio-inspired structural composites with desired properties (Silva et al., 2006; Wegst et al., 2015; Habibi et al., 2015). Hence, in-depth understanding of the interplays between the structure and mechanical properties of the complex biological system of bamboo is

* Corresponding author at: Department of Mechanical and Biomedical Engineering, City University of Hong Kong, 83 Tat Chee Avenue, Kowloon, Hong Kong. Tel.: +85234424061.
E-mail address: yanglu@cityu.edu.hk (Y. Lu).
[1] Present address: Department of Mechanical Engineering, University of Michigan, 2350 Hayward Street, Ann Arbor, Michigan, USA.

http://dx.doi.org/10.1016/j.mechmat.2016.03.002
0167-6636/

at the heart of producing futuristic materials with tunable properties (Silva et al., 2006; Habibi et al., 2015; Habibi and Lu, 2014; Huang et al., 2012; Low et al., 2006; Obataya et al., 2007; Shao et al., 2009; Tan et al., 2011; Wegst, 2008). Among the remarkable mechanical characteristics, it is expected that structural bamboo material shall also exhibit a reasonable viscoelastic behavior, even in dehydrated/desiccated condition, given that it is mainly constituted by natural polymers: bamboo's both major microstructural constituents (fibers and parenchyma cells) are lamellar composites consisting of cellulose microfibrils (40–50 wt. %) embedded in a lignin (20–30 wt. %) and hemicellulose (15–28 wt. %) matrix, in which minor amounts (5–10 wt. %) of extractives, such as, waxes and gums are also present (Wegst, 2008; Jain et al., 1992; Li et al., 2010; Li et al., 2011; Li et al., 2015).

Pertaining to the ability of adopting bamboo as an excellent biomimetic template (Wegst et al., 2015), it is also essential to understand the viscoelastic damping behavior of bamboo, since it could provide a noteworthy insight on its high impact energy fracture (Yamashita et al., 2001). In addition, from the structural point of view, viscoelastic damping could minimize the airborne noise radiation in vibrating condition by converting the energy to heat, which distributes within the structure itself (Sewda and Maiti, 2013). Although quite a few studies have been carried out so far, to explain the viscoelasticity in other biological structural materials, such as processed wood (Jiang et al., 2010; Zhang et al., 2012), bone (Yamashita et al., 2001; Shepherd et al., 2011), etc., there remain very few attempts which had been made to dedicatedly investigate the viscoelastic behavior of structural bamboo as a unique functionally-graded hierarchical cellular material. In an early attempt by Amada et al. (Amada and Lakes, 1997), the viscoelastic damping behavior of raw bamboo at different humidity levels was investigated and it was found that bamboo culm demonstrated larger damping coefficient in the course of torsion than during bending. However, it appears that the role of environmental impacts such as humidity, temperature and etc., on the macroscopic viscoelastic behavior of bamboo culm and other biological materials has been given considerable attention to, whereas the contributions from their respective microstructural phases alongside the underlying mechanisms at molecular level have been less studied. Direct experimental investigation of single bamboo fibrils is relatively recent and made possible with the use of micro-tensile testing system, which allows to assess the effect of moisture content on the creep behavior of bamboo fibers at fibril level (Yu et al., 2011). Although the viscoelastic properties of bulk bamboo and the fibers could be directly related to the lamellar structure and to the basic building blocks, including cellulose, hemicellulose and lignin, there is still no clear understanding on the role of these building blocks in affecting the bamboo's overall mechanical properties.

Hence, in this work we aimed to investigate the macroscopic viscoelastic damping behavior of desiccated bulk bamboo alongside the viscoelasticity of its individual microstructural constituents at ambient temperature. Along with the macro and micro-scale evaluation, the viscoelastic behavior of single molecules of bamboo's major building blocks was also evaluated in a holistic approach, to unveil the intrinsic viscoelasticity (without considering the environmental factors, e.g. moisture content) of bamboo's microstructural constituents alongside their interplays within bamboo's hierarchical structure as well as to assess the molecular origins of the exhibited viscoelastic behavior. Together with the experimental and computational inputs, a phenomenological viscoelastic model, comprising a Hookean spring and a Maxwellian linear viscoelastic unit, shall be then developed to further interpret the hierarchical structure-induced viscoelasticity in bulk bamboo structure.

2. Samples and methods

The samples were collected from mature Moso or "Mao Zhu" bamboo (*Phyllostachys edulis* species, from Jiangsu and Zhejiang provinces in China, ~5 years old) and were dehydrated with ethanol and were kept at vacuumed desiccators for few days prior to the study to minimize their humidity content. Dehydrated specimens have been used in order to maintain the focus of the study on the intrinsic viscoelasticity from bamboo's hierarchical microstructure, rather than repeating those earlier efforts dealing with humidity and other environmental contributions.

To quantify the viscoelastic damping behavior of bulk bamboo, small cubic samples ($8 \times 8 \times 8\,mm^3$) were subjected to dynamic compressive sinusoidal loading (frequency (f): 0.1, 1.0, 10.0 and 100.0 Hz) along their longitudinal direction (LD) at displacement control mode (amplitude: ~0.04 mm), at ambient temperature, utilizing a MTS 370 (Servo) Axial Torsional Material Testing System (see Fig. 1a–c). To ensure that the sinusoidal loading experiments were conducted in the elastic regime of bulk bamboo, similar cubic samples were subjected to a few monotonic compressive experiments, at the outset, to get a basic insight on the elastic regime of bulk bamboo under compression.

To explore the localized viscoelastic behavior of individual microstructural constituents of bamboo, load-controlled (maximum load: 600 μN) nano-indentation experiments were conducted dedicatedly on the carefully polished surfaces of microscopic structural phases (viz. individual bamboo fibers and parenchyma cell walls, respectively) (see Fig. 1d), by utilizing a Hysitron TI-750 Ubi™ machine with a calibrated Berkovich tip (radius ~200 nm). The schematic diagram of a typical load function, which was adopted here, is displayed in Fig. 1f. The load functions consisted of a loading segment (duration: t_l) followed by a holding segment (duration: t_h) and thereafter an unloading segment (duration: t_u). In order to configure different loading functions, a fixed t_l of 10 s was used, with varying t_h and t_u within the ranges of 0–5 s and 3–7 s, respectively. For each load function, 30 indentation experiments were conducted on fibers and parenchyma cells at different locations.

To assess the viscoelastic behavior of bamboo at molecular level, constant force Steered Molecular Dynamic (SMD) simulation was applied to the molecules of major building blocks of bamboo structure, including crystalline cellulose, amorphous hemicellulose and amorphous lignin

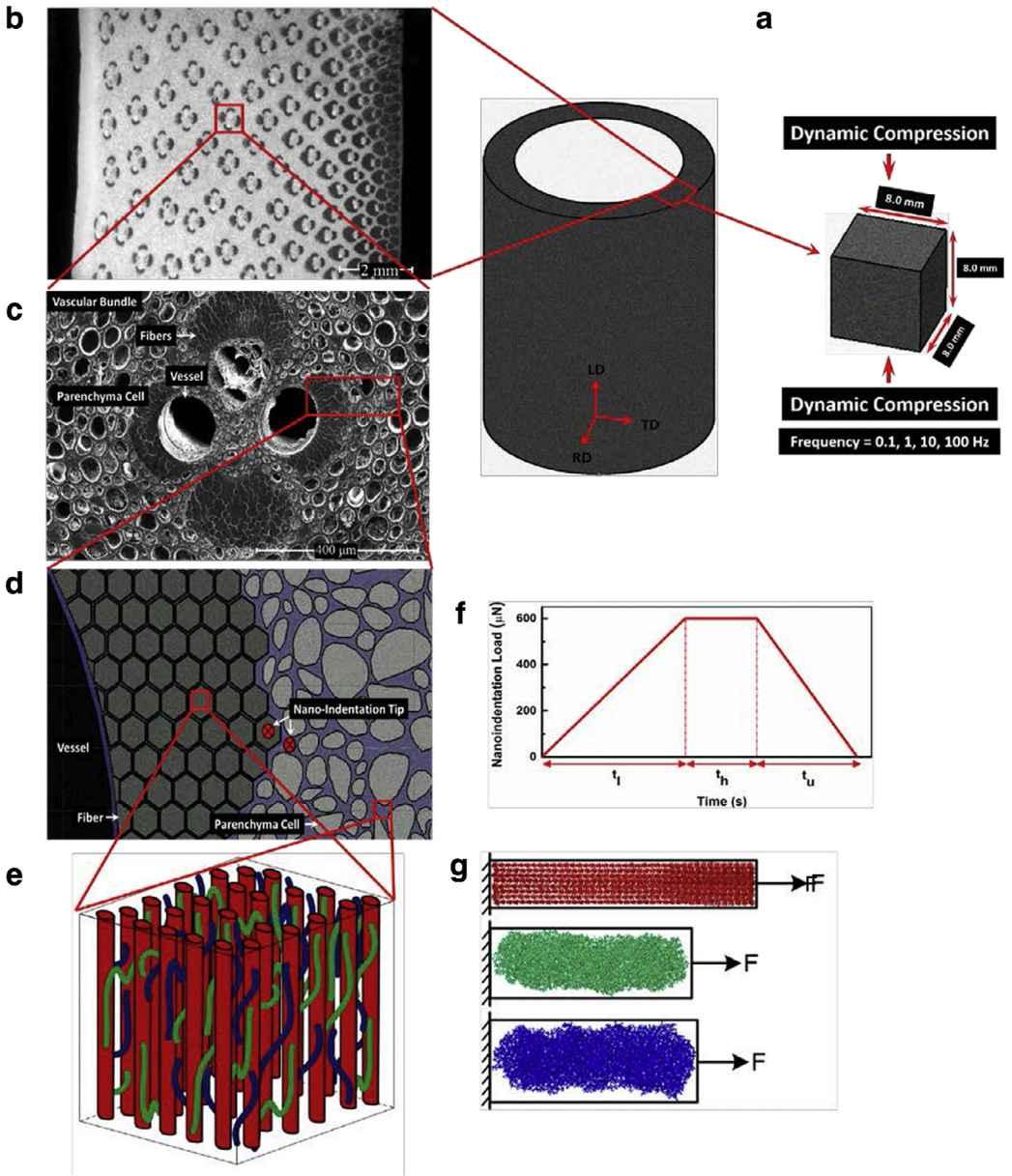

Fig. 1. Samples and experimental configuration: (a) schematic representation of dynamic compression with respect to (b–c) dehydrated bamboo culm along with (d) nano-indentation experiments on bamboo's microstructural constituents (fibers and parenchyma cells), and (e) bamboo cell wall structure at molecular level. In the (f) load function which was adopted during the indentation experiment, t_l was fixed to the value of 10 s; whereas t_h and t_u were varied within the ranges of 0–5 s and 3–7 s, respectively. The snapshots of the equilibrated molecules of crystalline cellulose (in red), amorphous hemicellulose (in green) and amorphous lignin (in blue), subjected to computational creep tests, are displayed in (g). (For interpretation of the references to colour in this figure legend, the reader is referred to the web version of this article.).

(see Fig. 1e), which were subjected to computational creep tests along their principal axis. The crystalline cellulose I_β has been found to be predominant in bamboo (Sun et al., 2008), and accordingly was chosen as the representative cellulose model here. The crystalline cellulose model was constructed by using the cellulose-builder program (Gomes and Skaf, 2012); given that it had 36 chains, where each chain consisted of 40 covalently bonded glucose rings. The cellulose molecule had an approximate length of 21 nm and a thickness of 3 nm, close to the earlier reported values (Wang et al., 2012). To construct a hemicellulose molecule model, meanwhile, hemicellulose of the xylem type is used as a representative since it was reported to be abundant in bamboo (Maekawa, 1976). The amorphous hemicellulose model was constructed from a unit cell containing 65 hemicellulose segments, which consisted of 35 segments with 5 D-xylopyranosyl residues, bonded covalently, and additional 30 segments with L-Arabinofuranosyl (Araf) connected to the third xylosyl residues by α-(1-3) linkage (Charlier and Mazeau,

2012; Jin et al., 2015). The segments were added in sequence with random orientation while an equilibration was carried out after each adding step (Jin et al., 2015). The unit cell was replicated in length to generate the hemicellulose molecule, which had an approximate length of 17 nm, a thickness of 5 nm, and approximately 30,000 atoms, as close to the cellulose model. Unlike cellulose and hemicellulose, for the amorphous lignin molecules, various monomeric units and linkages between the units were observed (Wen et al., 2013). Particularly, it was reported that the syringyl (S) unit and the linkage of type β-O-4 were most common in bamboo structure. In the first approximation, the S unit and the β-O-4 linkage were included. The lignin model was constructed three-dimensionally by forming the β-O-4 linkages between the S units, which was achieved by modifying a dynamic bond-forming algorithm developed in earlier study (Tam and Lau, 2014). The polymerized network was replicated in length to build a lignin molecule with approximately 30,000 atoms, as similar to cellulose and hemicellulose models.

Molecular dynamics simulations were performed using the LAMMPS code (Plimpton, 1995), along with the Polymer Consistent Force Field (PCFF) (Sun et al., 1994; Sun, 1995), which is suitable for different types of polymeric materials and was already validated in studying the crystalline and amorphous structures of cellulose (Mazeau and Heux, 2003; Tanaka and Iwata; 2006), and the interactions between cellulose and other different materials, such as hemicellulose, aromatic compounds, and graphene (Hanus and Mazeau, 2006; Da Silva Perez et al., 2004; Rahman et al., 2013). For the pair–wise interactions, the truncation method of finite cutoff distance has been used effectively to study the viscoelastic properties of polymers and collagen molecules (Cifre et al., 2004; Simoes et al., 2006; Gautieri et al., 2012). It could be learned that the long-interactions would not contribute to significant variation in simulation results, though they are commonly used in the MD simulations. As the investigated bamboo building blocks are essentially polymer materials, similar technique could be used for studying their viscoelastic behavior. And thus, van der Waals and Columbic interactions were computed using a cutoff distance of 1.35 nm for neighbor list. Rigid bonds were applied to constrain the lengths of covalent bonds involved hydrogen atoms. Non-periodic and shrink-wrapped boundary conditions were used in all three dimensions during the simulations. The energy minimization was carried out by adopting the steepest descent algorithm until the convergence. The molecules were then equilibrated under the canonical ensemble at a temperature of 300 K with a Nosé–Hoover thermostat (Gautieri et al., 2012). Under the applied boundary condition, the system could expand or shrink during the equilibration, as similar to the equilibration process containing a series of NVT-NPT dynamics. The equilibration was run for 20 ns with a time step of 1 fs. The root mean square displacement (RMSD) of the atoms reached a stable value before the equilibration run got completed, which implied that the molecules were equilibrated properly. After the structural equilibration, computational creep test was carried out. During the constant force SMD simulation, one end of the molecule was kept fixed whereas the other end was subjected to an instantaneous constant force (the loading configurations of the three molecules are shown in Fig. 1g). The total applied force was 25 and 50 nN on the cellulose molecule, 2 and 3 nN on the hemicellulose molecule, and 1.5 and 1.8 nN on the lignin molecule, respectively. As non-periodic and shrink-wrapped boundary conditions were used in all three dimensions during the simulations, the molecule could response instantaneously under the externally applied force. The instantaneous stress σ_0 was finally calculated by dividing the applied force by the cross-sectional area of the molecule, which was determined from the molecules after the equilibration. The adopted simulation setup could mimic a single molecule test, where an instantaneous load was applied to the molecule and the strain response in time could be obtained. The creep test simulations were run under the canonical ensemble for 5 ns in the case of cellulose molecule and 10 ns in the cases of hemicellulose and lignin molecules, which were found long enough to reach deformation in equilibrium (Gautieri et al., 2012).

3. Results and discussions

3.1. The hierarchical structure of bamboo

As demonstrated in our earlier study (Habibi and Lu, 2014), bamboo culm is indeed an optimized fiber reinforced composite with cellular parenchyma as the matrix. Parenchyma cells ($57.3 \pm 2.5\%$, in vol. %) constitute the majority of bulk bamboo, whereas fibers ($37.1 \pm 3.3\%$) and hollow vessels ($5.6 \pm 0.8\%$) make up the rest. Both parenchyma cells and fibers exhibit a size distribution in terms of their radial and longitudinal dimensions, namely diameter (D) and height (H)/length (L), respectively. The effective diameter of the parenchyma cells was found to be within the range of $D_p = 40–50\ \mu m$ (see Fig. 2a), whereas fibers have an effective diameter within the range of $D_f = 8–12\ \mu m$ (see Fig. 2c) (the subscripts 'p' and 'f' represent parenchyma cells and fibers, respectively). The height of the parenchyma cells along with the length of the fibers were also observed to be within the range of $H_p = 30–70\ \mu m$ (see Fig. 2b) and $L_f = 200–300$ mm (see Fig. 2d), respectively.

At the lowest hierarchical scale of bamboo, parenchyma cells and fibers mainly consist of cellulose microfibrils embedded in a hemicellulose and lignin matrix (Wegst, 2008; Jain et al., 1992). To investigate the bamboo's viscoelasticity at the molecular level, the modeled unit cells should be close to those found in a real system. Density (ρ) is a good physical property for evaluating, if the constructed conformations are close to the reality. In the last 5 ns equilibration run under canonical ensemble, the densities of the constructed molecules are recorded and averaged. The final equilibrated conformations of cellulose, hemicellulose and lignin have average densities of $1.58 \pm 0.002\ g/cm^3$, $1.59 \pm 0.001\ g/cm^3$ and $1.48 \pm 0.001\ g/cm^3$, respectively. These are comparable with experimental data as shown in Table 1. In comparison to the literature, the simulated ρ of cellulose molecules

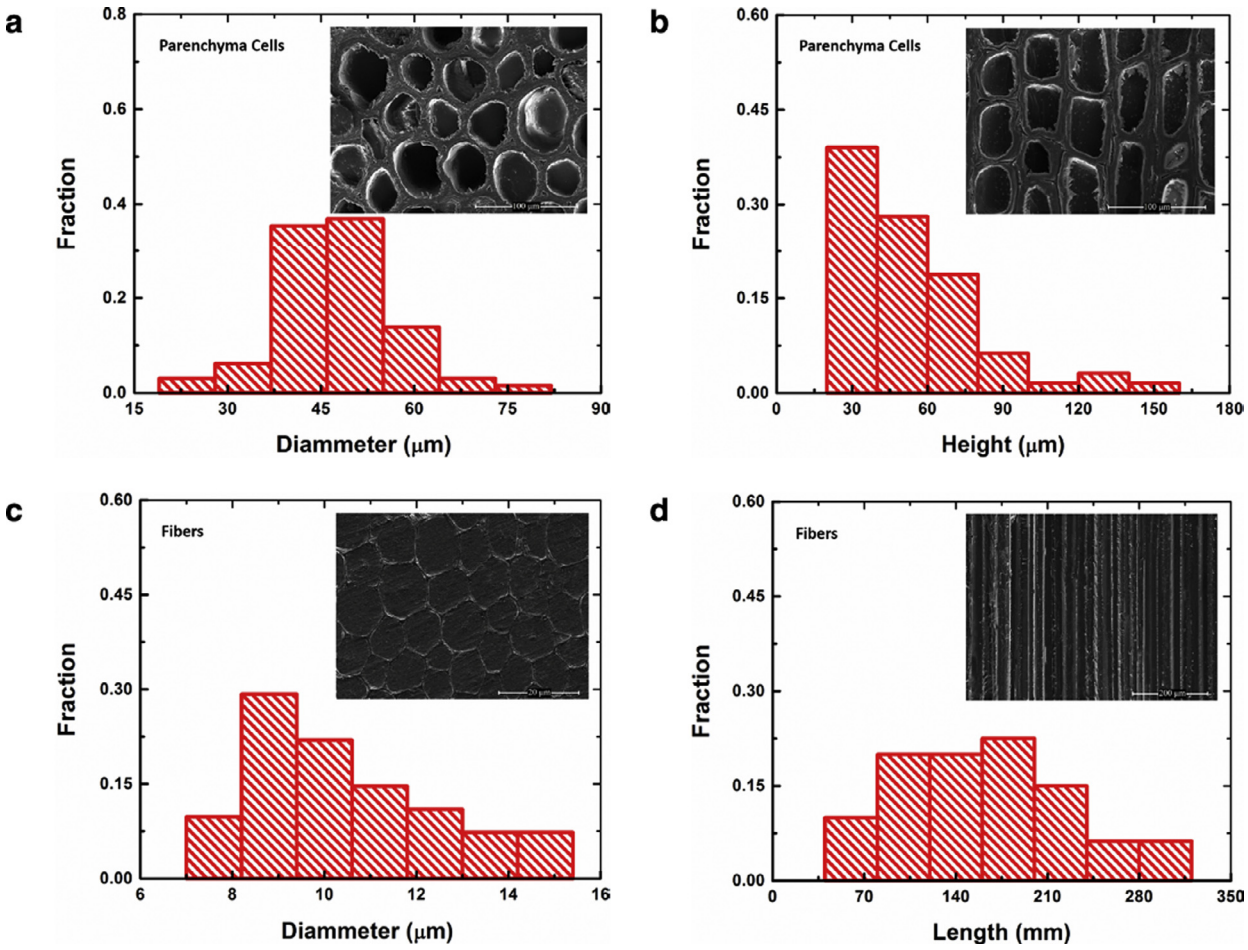

Fig. 2. Morphology and size distribution of bamboo's major constituents: size distribution and SEM micrographs of (a–b) parenchyma cells and (c–d) bamboo fibers, in the transverse and longitudinal directions, respectively. Note: to acquire the size distribution of either fibers or parenchyma cells, almost six micrographs, taken from different parts of the bamboo culm, were used in the image processing.

Table 1
Density (g/cm^3) of cellulose, hemicellulose and lignin obtained from the molecular calculations and experiments.

Material	Simulation	Experiment
Cellulose	1.58 ± 0.002	1.45–1.59 (Gibson, 2012), 1.65 (Youssefian and Rahbar, 2015)
Hemicellulose	1.59 ± 0.001	1.52 (Youssefian and Rahbar, 2015)
Lignin	1.48 ± 0.001	1.20–1.25 (Gibson, 2012), 1.33 (Youssefian and Rahbar, 2015)

provides an excellent agreement, while the hemicellulose and lignin molecules overestimate the real densities by 4.6% and 11.2%, respectively. The slight discrepancies could be partly resulted due to the fact that the models are simulated in a vacuum condition which does not match precisely with the experiments (Youssefian and Rahbar, 2015). In view of the good agreement of ρ with experiments, the generated models of cellulose, hemicellulose and lignin molecules could be regarded as reasonable representatives of the real structures.

3.2. Viscoelastic behavior of bulk bamboo structure

In view of the structural features of bamboo vis-à-vis a dynamic compressive loading, it was demonstrated that the deformation in the elastic regime of the dehydrated bulk bamboo structure, at ambient temperature, remains viscoelastic (see Fig. 3). At relatively low loading frequency (f: 0.1; see Fig. 3a), bamboo culm exhibited nearly elastic behavior as in quasi-static test. However, as the loading frequency increased, a mechanical hysteresis loop started to emerge, which expanded monotonically with further increase in loading frequency f: 1.0–100 Hz (see Fig. 3b–d). The disclosed viscoelasticity could be also inferred with reference to the stress (t)–strain (t) curves, which are displayed in Fig. 4. As demonstrated, in the case of low frequency dynamic compression tests, the phase lag amongst the applied stress signal and its corresponding recorded strain was negligible. However, as the loading frequency increased, the phase lag started to develop, which could be also verified with the exhibited hysteresis loop's expansion in the stress–strain curves (see Fig. 3). In an elastic material, the stress and strain signals remain in phase, i.e.,

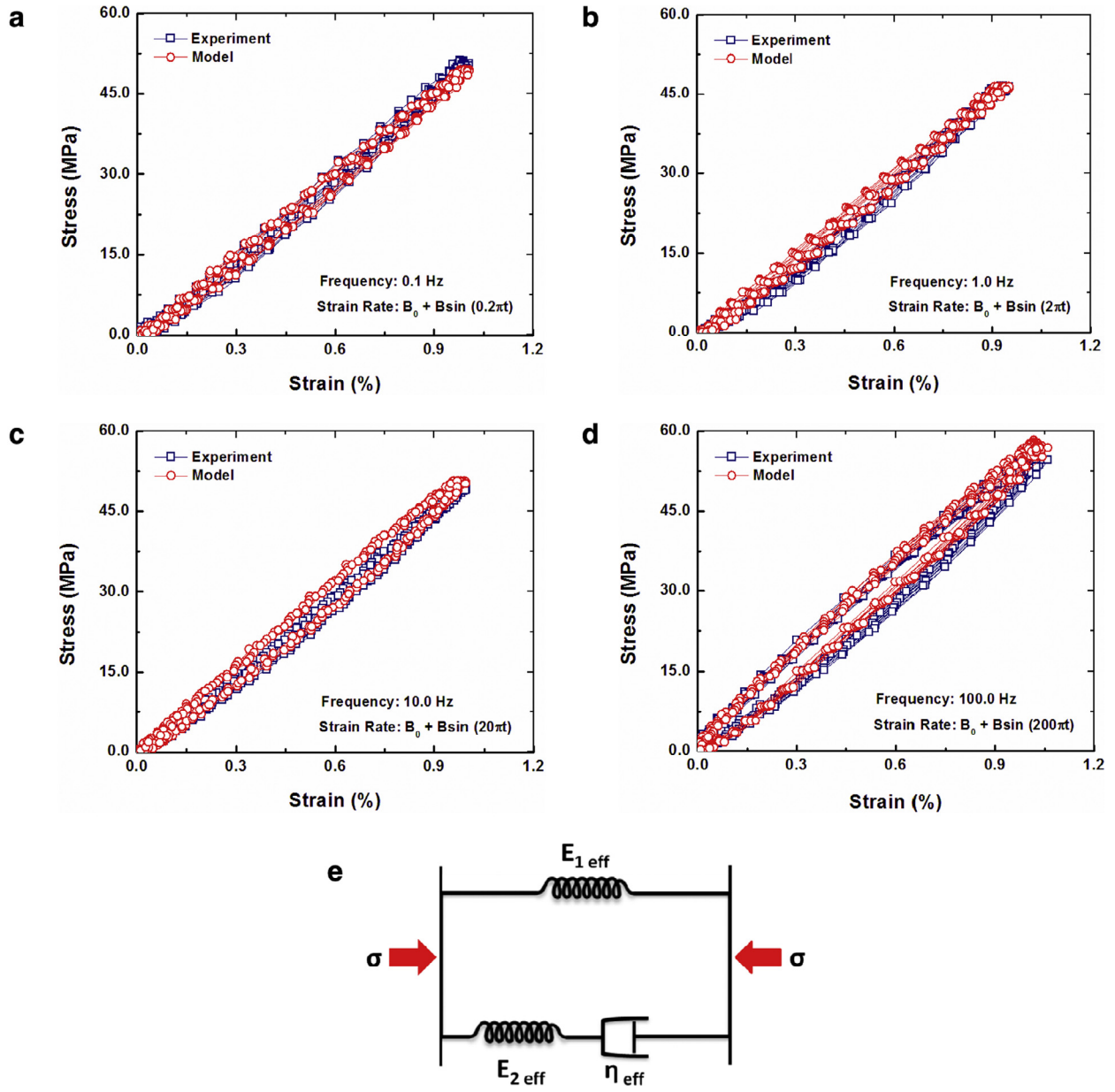

Fig. 3. Mechanical hysteresis in dynamic compression tests: (a–d) the experimental results of dynamic compression tests (frequency: 0.1, 1.0, 10.0 and 100.0 Hz) showing the mechanical hysteresis developed at high strain rates, alongside the results from the (e) adopted phenomenological viscoelastic model. In the strain rate equations, B_0 and B are constant where t stands for time in second.

response occurs instantaneously, whereas in a viscoelastic material, there is a phase difference or equivalently a time lag between the applied stress signal and its recorded corresponding strain, which arises from the time taken for molecular rearrangement (Sewda and Maiti, 2013).

Here, the in-phase component represents the storage modulus of the structure and can be denoted by $E' = E_0 \cos \delta$, whereas the out-phase component stands for the loss modulus which is indicated by $E'' = E_0 \sin \delta$ (the 'E_0' and 'δ' stand for the elastic modulus and the phase lag between the stress and strain signals in radian, respectively). The damping ratio, which gives the ratio between the out-phase (viscous) and the in-phase (elastic) component is also represented by $\zeta = \frac{1}{2}\ (\tan\delta = \frac{E''}{E'})$ (Poletto et al., 2012). Interestingly, it was demonstrated that the storage modulus E', which indicates the inherent stiffness of the bulk structure of bamboo, is almost loading frequency independent (~6.0 GPa), whereas the loss modulus E'', which stands for the energy dissipation owing to the internal friction, is noticeably loading frequency dependent (see Fig. 5a). At very low loading frequencies (i.e., 0.1–1.0 Hz), the E'' was almost around ~0.3 GPa, whereas it kept increasing with increase in loading frequency and ultimately reached ~1.2 GPa at f: 100.0 Hz. Parallel with loss modulus

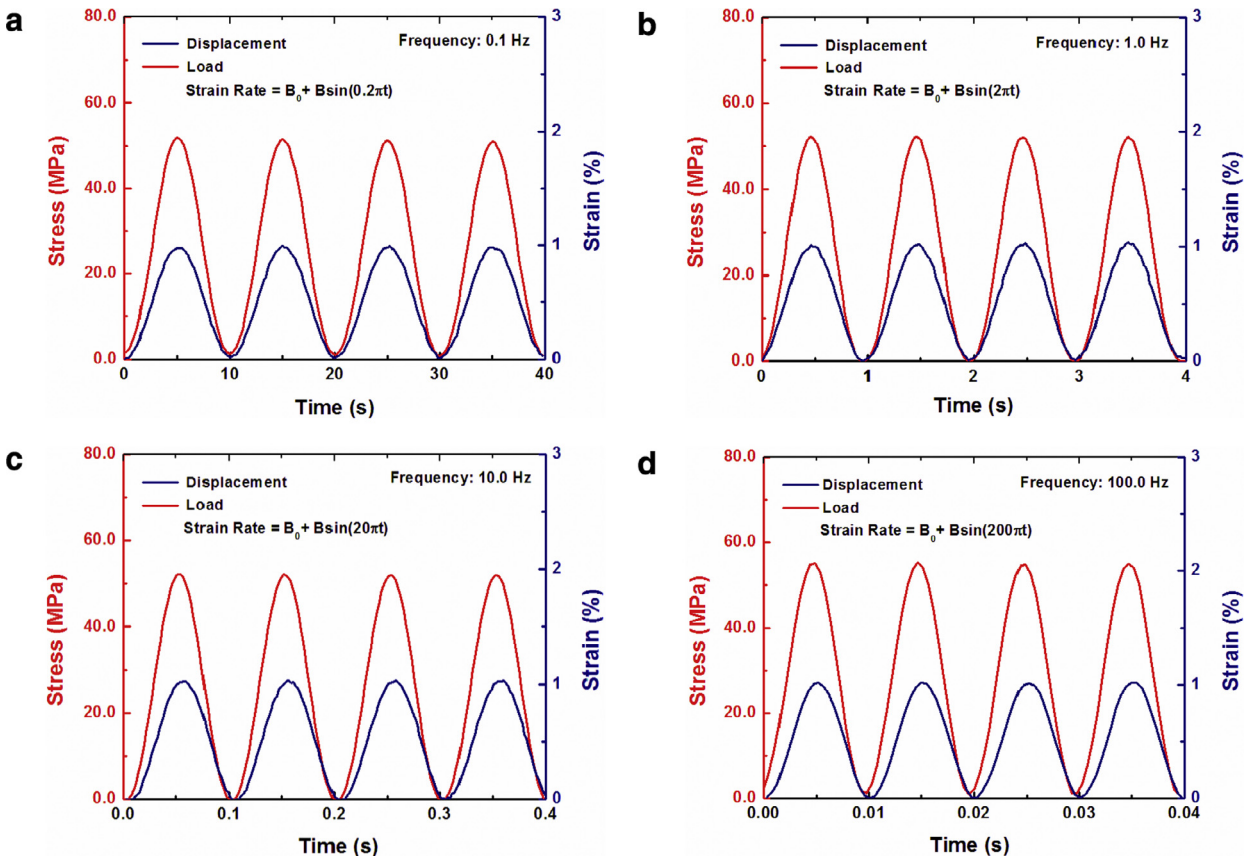

Fig. 4. Stress–strain phase lag in dynamic compression tests: (a–d) the experimental results of dynamic compression tests (frequency: 0.1, 1.0, 10.0 and 100.0 Hz) demonstrating the phase lag or equivalently time lag amongst the applied stress signal and its recorded corresponding strain. The stress and strain spectra collected at different strain rates are keyed to the stress–strain curves shown in Fig. 3. In the strain rate equations, B_0 and B are constant where t stands for time in second.

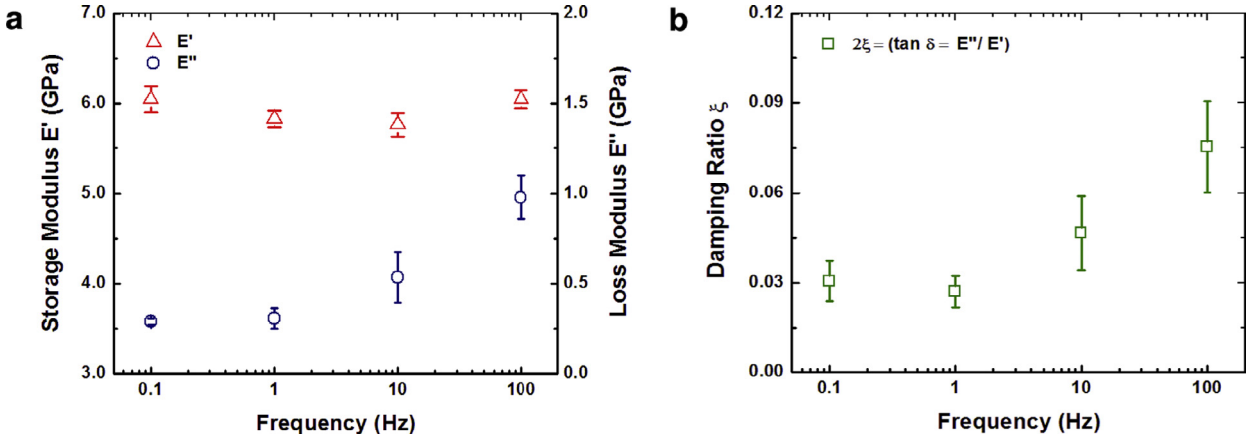

Fig. 5. Viscoelasticity in dehydrated bulk structural bamboo material at ambient temperature: variation of (a) storage E' and loss E'' modulus along with (b) damping ratio in bulk structure of bamboo as a function of loading frequency. Note: the storage modulus (E') indicates the inherent stiffness of the bulk structure of bamboo, whereas the loss modulus (E") stands for the energy dissipation owing to internal friction.

variation, the damping ratio of the bamboo also improved with increase in loading frequency and ultimately reached the value of ~0.08 at f: 100.0 Hz (see Fig. 5b). It is noted that all E', E", and ζ values were calculated based on $E_0 = \sim 6.3$ GPa, which was extracted from the monotonic compression tests conducted earlier.

3.3. Viscoelastic model for hierarchical bio-composites

In the light of the exhibited macroscopic viscoelastic damping behavior, the dehydrated bulk bamboo structure could be regarded as a viscous liquid-like phase enveloped by an elastic solid-like part. Note that, here the

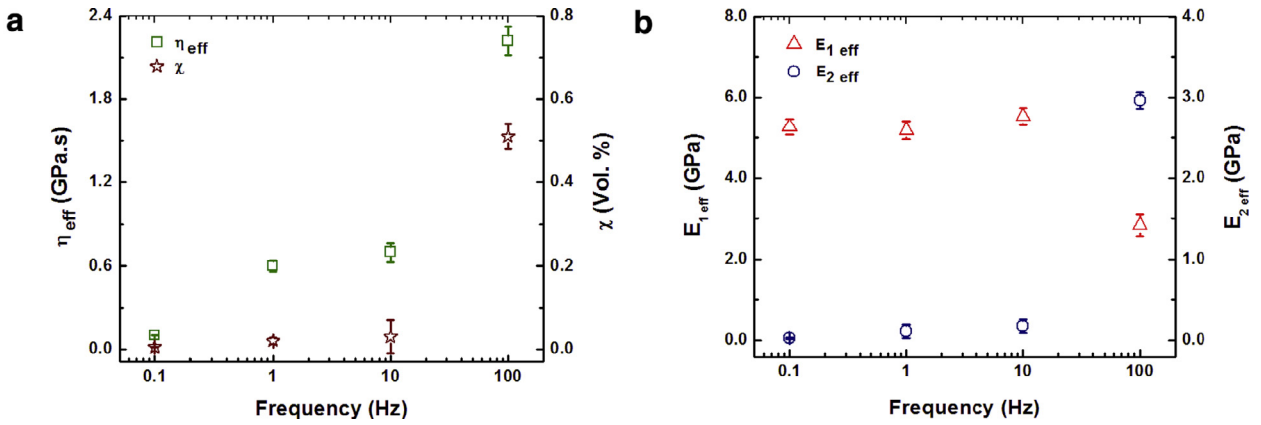

Fig. 6. Phenomenological viscoelastic model for structural bamboo material: variation of (a) effective viscosity as well as volume fraction of detected viscous phases along with (b) $E_{1\text{eff}}$ and $E_{2\text{eff}}$, evaluated by the adopted viscoelastic model, with loading frequency.

"liquid-like" phase does not consider the contribution of humidity. The physical description along with the governing equation for such a phenomenological model is demonstrated in Fig. 3e and Eq. (1), respectively, given that the viscous phase is analogically considered to be the Maxwellian model, whereas the elastic part is regarded to be the elastic spring (Huo et al., 2012; Huo et al., 2013). The relationship among stress, strain, strain rate, and relevant parameters is demonstrated by the following differential equation (Huo et al., 2012):

$$\sigma = E_{1\,\text{eff}}\,\varepsilon - \frac{\eta_{\text{eff}}}{E_{2\,\text{eff}}}\frac{\mathrm{d}\sigma}{\mathrm{d}t} + \eta_{\text{eff}}\frac{E_{1\text{eff}} + E_{2\text{eff}}}{E_{2\text{eff}}}\frac{\mathrm{d}\varepsilon}{\mathrm{d}t} \tag{1}$$

where σ, ε and t represent stress, strain, and time, respectively, $E_{1\,\text{eff}}$ and $E_{2\,\text{eff}}$ are the effective elastic moduli in Hookean spring and the elastic component in the viscoelastic model, respectively, and η_{eff} denotes the effective viscosity of the viscoelastic model. Here, $E_{1\text{eff}}$ is the modulus which mainly corresponds to elastic deformation of the backbone of bamboo structure, whereas $E_{2\text{eff}}$ is the modulus which is related to the elastic spring and corresponds to the bamboo's viscoelastic phase. Since, $E_{1\,\text{eff}}$, $E_{2\,\text{eff}}$ and η_{eff} are the effective parameters of individual parts to the whole unit, we can redefine these parameters as $E_{1\ \text{eff}} = (1-\chi)E_0$, $E_{2\ \text{eff}} = \chi E_0$ and $\eta_{\text{eff}} = \chi\eta$. Here E_0 is the elastic modulus of the bulk bamboo, η is the averaged viscosity and χ is the volume fraction of the viscous phase in bulk structure of bamboo.

The phenomenological Eq. (1), pertaining to the model shown in Fig. 3e could be therefore represented by the following differential equation (Huo et al., 2012):

$$\sigma = (1-\chi)E_0\epsilon - \left(\frac{\eta}{E_0}\right)\dot{\sigma} + \eta\dot{\epsilon} \tag{2}$$

Here $\epsilon = \epsilon(t)$ represents the input strain function and $\sigma = \sigma(t)$ represents the output stress function. The 'dot' symbol on the parameters also represents their first order time derivatives. The input strain function used in the experiment is of the form: $\epsilon(t) = B_0 + B\sin(\omega t + \phi)$, where B_0 and B are constant, $\omega = 2\pi f$ is the angular frequency and ϕ is the phase angle. Values of these input parameters were evaluated by performing least-square fitting to the ϵ versus t data obtained in the experiment. Eq. 2 could be solved by using Laplace transformation method (see *Supplementary Material*) and the general solution for the Eq. 2 appears as the following form:

$$\sigma(t) = A_0 + A\sin(\omega t + \phi + \delta) + A'\exp\left(-\frac{E_0 t}{\eta}\right) \tag{3}$$

where, $A_0 = (1-\chi)\,BE_0$, $A = \frac{p}{\Delta}$, and $A' = [E_0B_0\chi + \sigma_0 - E_0\epsilon_0 - \frac{E_0^2B\chi}{\sqrt{\Delta}}\cos(\phi+\theta)]$, with $M = E_0B(E_0^2\chi' + \eta^2\omega^2)$, $\mathrm{N} = \chi E_0^2B\eta\omega$, $(\chi' = 1-\chi)$ and, $p = \sqrt{N^2+M^2}$, $\Delta = E_0^2 + \eta^2\omega^2$, $\delta = \tan^{-1}(\frac{N}{M})$, $\theta = \tan^{-1}(\frac{E_0}{\eta\omega})$. Note that as time progressed, the contribution from the time dependent terms became less significant and the output stress function appeared to be a sinusoidal function with a phase shift δ, which is again a function of the input parameters, and the structural and mechanical properties of the material. It is disclosed that the exponential decay term in the Eq. (3) plays an important role particularly in the low-frequency regime (0.1–1.0 Hz) of the input strain functions. This could be justified by the fact that, in the low frequency regime, the time duration between two subsequent input strain-values is comparatively larger, which allows relatively more time for the relaxation of the stress, thereby making the exponential decay term more significant.

By comparing the experimental and the fitting curves, given in Fig. 3a–d, one can see that the adopted model along with suitable fitting parameters reasonably explain and capture the mechanical hysteresis as well as the structural features of the deformation units of bulk structure of bamboo, respectively, in both low and high frequency domains. Unlike the cases where the fitting parameters are independent of the stress rate, the χ and η in the case of bamboo were strain rate dependent. As displayed in Fig. 6a, the χ (volume fraction of viscous phases) in bulk bamboo is a function of loading frequency, given that it was roughly ~0.005 at the lowest loading frequency (f: 0.1 Hz) while it started to increase with loading frequency and eventually reached ~0.5 at f: 100.0 Hz. Similarly, at f: 0.1 Hz, the extracted η was in the range of ~0.1 GPa.s,

whereas it increased with loading frequency and eventually reached ~2.0 GPa.s at f: 100.0 Hz.

From the perspective of the applied stress, the elastic components in Hookean spring ($E_{1\text{eff}}$) and in Maxwellian model ($E_{2\text{eff}}$) with the viscous phase also behave differently upon the applied stress (see Fig. 6b). As demonstrated in Fig. 6b, at low and moderate loading frequencies (f: 0.1, 1.0 and 10.0 Hz), the $E_{1\text{eff}}$ stayed almost stable at ~5.2 GPa, which is pretty close to the storage modulus of the bulk bamboo (see Section 3.2; Fig. 5a), whereas it abruptly decreased to ~2.84 GPa as loading frequency increased to 100 Hz. Similarly, $E_{2\text{eff}}$ remained almost consistent at around ~0.03–0.17 GPa at f: 0.1–10.0 Hz, respectively, whereas it abruptly increased to ~3.0 GPa as loading frequency jumped to f: 100 Hz. Regarding the observed behavior, it is noted that, as far as a dynamic loading is concerned, the stress on the phenomenological model can be represented by:

$$\sigma = \sigma_1 + \sigma_2 \tag{4}$$

where σ_1, σ_2 denotes the applied stress on the Hookean spring and the Maxwellian body, respectively. As the frequency of the applied load increases, the bulk bamboo becomes more viscous, i.e. the viscous behavior of the phenomenological model becomes pronounced, and accordingly σ_2 increases while σ_1 decreases, which leads to an increase in $E_{2\text{eff}}$ and η_{eff} along with the decrease in $E_{1\text{eff}}$. However, despite of tremendous variation in $E_{1\text{eff}}$ and $E_{2\text{eff}}$ with increase in loading frequency, their summation keeps at a relatively constant level, which concludes that the elastic portion within the bulk bamboo remains largely undamaged. Moreover, though the volume fraction of viscous phases (χ) in bamboo structure gets pronounced, once the loading frequency reached above a certain threshold, the growth does not break down the elastic portion of the structure.

3.4. Viscoelastic behavior of bamboo's microstructural constituents

To unveil the intrinsic microstructural mechanisms responsible for the exhibited viscoelasticity in bulk bamboo, viscoelasticity of bamboo's microstructural phases were characterized by utilizing local nano-indentation experiment. At the outset, the nano-indentation results, achieved by using load functions comprised of a fixed t_l followed by different t_h and t_u, were processed via Oliver–Phar method, Eq. (5), to calculate the tip-sample reduced moduli E_r (Ngan and Tang, 2002).

$$E_r = \frac{\sqrt{\pi}}{2}\frac{S}{\sqrt{A_c}} \tag{5}$$

where S is the contact stiffness at the onset of unloading and A_c is the contact area at the full loading, not the residual indentation area after the unloading. A_c is calculated from the contact depth, h_c, by assuming the shape function of the indenter which is given in Eqs. (6–7) (Ngan and Tang, 2002; Feng and Ngan, 2002). In Eq. (7), ϵ is a constant depending on the indenter geometry, which is 0.75 for Berkovich tip (Feng and Ngan, 2002) and P_{max} stands for the maximum load which was 600 μN here.

$$A_c = f(h_c) \tag{6}$$

$$h_c = h - \epsilon\frac{P_{max}}{S} \tag{7}$$

Here, owing to the concurrence of creep and elastic deformation in the course of the indentation (Feng and Ngan, 2002), the contact stiffness S, in both Eqs. (5) and (7) is not same as the apparent S_u (the slope of the unloading curve at the onset of unloading); but it is related to S_u through the relation given in Eq. (8) (Feng and Ngan, 2002). The second term in the right hand side of the Eq. (8) is the correction term owing to creep and thermal drift, given that h_h is the indenter displacement corresponding to the P_n and $\dot{P}$ is the unloading rate at the onset of unloading (Feng and Ngan, 2002). The load P at which the 'nose' appears in the unloading load–displacement (P–h) curve is denoted as P_n hereafter. As demonstrated in Fig. 7, the displacement continued briefly after the onset of unloading, and it passed through a maximum before decreasing, as the load dropped further. The final derived E_r (for each loading configuration) along with their corresponding $\dot{P}$ and P_n were eventually fitted into Eq. (9) (Feng and Ngan, 2002) to extract the viscosity parameter ($\frac{\sigma}{\dot{\varepsilon}}$) of both fibers and parenchyma cells.

$$\frac{1}{S} = \frac{1}{S_u} + \frac{h_h}{|\dot{P}|} \tag{8}$$

$$P_n - P_i = \frac{4\sigma|\dot{P}|}{3\dot{\varepsilon}E_r} \tag{9}$$

where, P_i is the constant offset load at zero unloading and stands for the stress induced by the friction, which has been ignored here (Feng and Ngan, 2002).

As demonstrated in Fig. 8a–b, P_n depended on the unloading rate in a series of independent indentations to the same peak load of 600 μN, using the same loading rate of 60 μN/s, but different holding times before the unloading (see Fig. 8a–b). As illustrated, for both fibers and parenchyma cells, P_n decreased with reduction in the unloading rate $|\dot{P}|$, at each holding time, so that from the slope of the P_n versus $|\dot{P}|$ plots, as mentioned earlier, the viscosity parameter of each phase was evaluated. Interestingly, it was observed that fibers and parenchyma cells exhibited absolutely different viscoelastic behavior, when they were subjected to similar loading configurations (see Fig. 8c–d). As displayed in Fig. 8c, fibers demonstrated a viscosity of ~2.0–3.6 GPa.s (values varied as the unloading rate changed) at $t_h = 0$–1 s, whereas their viscosity sharply diminished with further increase in the duration of the applied stress (i.e., t_h) and eventually reached the steady value of ~0.3–0.5 GPa.s at $t_h = 7$ s. This decreasing trend of viscosity with respect to stress duration is an indication of thixotropic property which could be found in certain shear thinning fluids. On the contrary, the parenchyma cells showed an opposite behavior with respect to stress duration, which is identified as the rheopectic property, given that their viscosity was observed to improve with increase in the duration of applied stress. As displayed in Fig. 8d, parenchyma cells

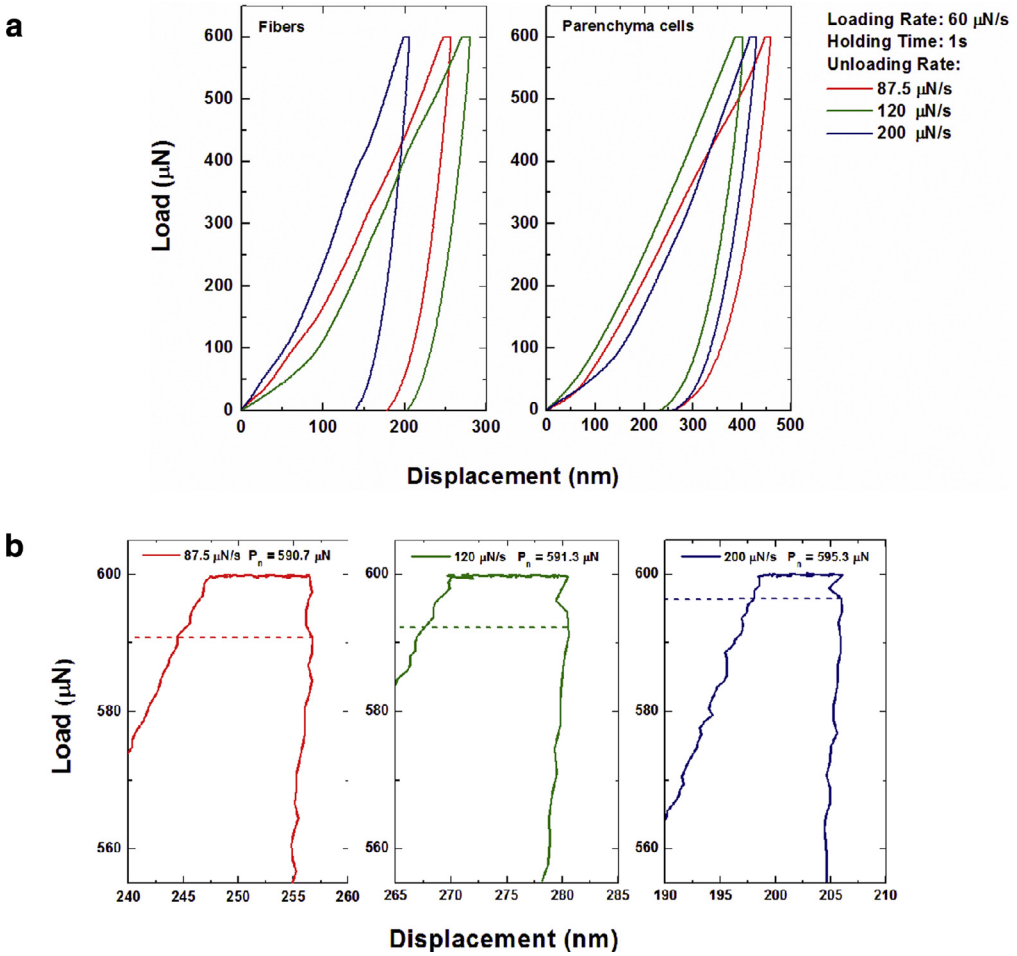

Fig. 7. Nano-indentation load–displacement (P–h) curves of (a) fibers and (b) parenchyma cells: all experiments had the same loading rate to the same peak load, same holding time but different unloading rates. (c–d) are the high magnifications of P–h curves revealing the occurrence of nose at the onset of unloading, selectively, in the case of fibers. Note: the maximum displacement in the unloading P–h curve is considered as nose here.

demonstrated a viscosity of ~1.8–3.0 GPa.s at $t_h = 0$–1 s, whereas their viscosity started to rise with increase in duration of applied stress and eventually reached ~3.0–7.0 GPa.s at $t_h = 7$ s. Once more, it is worth mentioning that, at a fixed duration of stress, a range for the viscosity is given here for both fibers and parenchyma cells, since their viscosity was found to be different at various unloading rates (see Fig. 8c–d).

3.5. Viscoelastic behavior of bamboo's molecular building blocks

Computational creep tests of cellulose, hemicellulose and lignin molecules were carried out by applying an instantaneous constant force and monitoring the engineering strain of each molecule over the time (see Fig. 9). It was demonstrated that the strain response in the case of cellulose molecule was time independent, which is a typical behavior of a Hookean spring (see Fig. 9a, d) and could be characterized by the Young's modulus, E. In the case of 25 and 50 nN loading conditions, the E of cellulose molecules was found to be 190 and 169 GPa, respectively, which is in a good agreement with the findings in earlier studies, as presented in Table 2 (Gibson, 2012; Youssefian and Rahbar, 2015). For the cases of hemicellulose and lignin molecules, their strain response showed a similar monotonic increase during the simulation timespan (see Fig. 9b–c), which is a typical behavior of the viscoelastic material with the Young's modulus E and the viscosity η being responsible for the elastic response and viscous behavior respectively. In order to determine the viscoelastic properties

Table 2
Young's Modulus (GPa) of cellulose, hemicellulose and lignin obtained from the SMD simulations and experiments.

Material	Simulation	Experiment
Cellulose	169, 190	120–140 (Gibson, 2012), 167 (Gibson, 2012), 90–200 (Youssefian and Rahbar, 2015)
Hemicellulose	4.3, 5.2	5.0–8.0 (Gibson, 2012), 3.5–8.0 (Youssefian and Rahbar, 2015)
Lignin	3.4, 4.8	2.5–3.7 (Gibson, 2012), 2.0–6.7 (Youssefian and Rahbar, 2015)

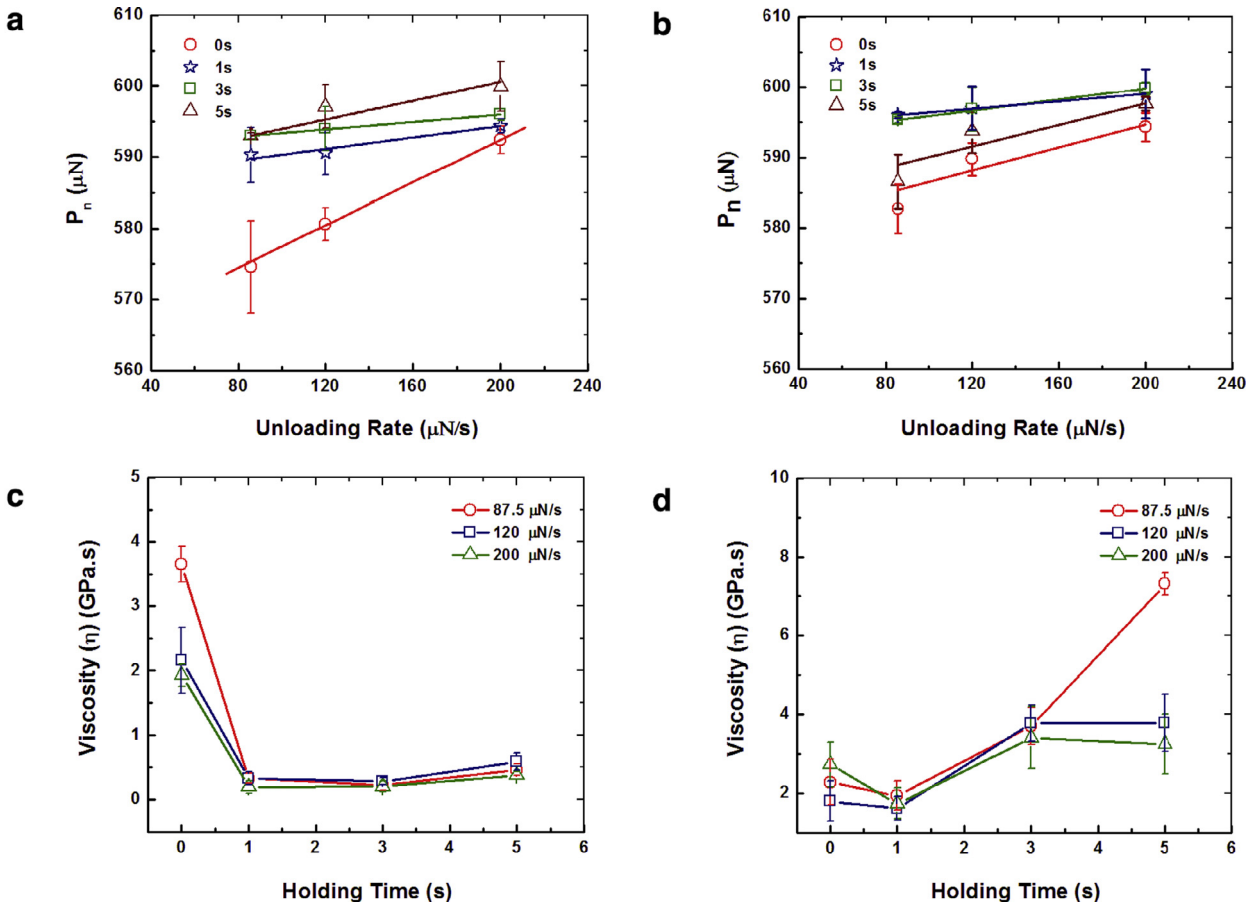

Fig. 8. Viscoelasticity in the microstructural constituents of bamboo at ambient temperature: effect of unloading rate ($|\dot{P}|$) on the load P_n (the load at which nose occurs in the P–h curves in the course of unloading) in the case of (a) fibers and (b) parenchyma cells. All experiments were done with same loading rate of 60 μN/s, but different holding times (0, 1, 3 and 5 s). (c–d): reveals the effect of holding time (stress duration) at the peak load on the viscosity parameter of (c) fibers and (d) parenchyma cells. The viscosity parameter is evaluated from the slope of P_n versus $|\dot{P}|$ plots shown in (a–b) and according to Eq. (5).

of the hemicellulose and lignin molecules, the Maxwellian model has been adopted to fit the strain–time data (see Fig. 9e). The first component in the equation, as shown in Fig. 9e, is the viscous creep deformation, which is proportional to the force and the time and can be revealed in the deformation of the dashpots; while the second component is related to the instantaneous deformation, which is proportional to the applied force initiated from the spring. For the loading conditions of 2 and 3 nN, E was found to be 5.2 and 4.3 GPa for the hemicellulose molecule respectively, which is pretty close to the earlier experimental studies, as illustrated in Table 2 (Gibson, 2012; Youssefian and Rahbar, 2015). Meanwhile, E of the lignin molecule was calculated as 4.8 and 3.4 GPa for the loading conditions of 1.5 and 1.8 nN respectively. In comparison with the experimental value, the simulated E of the constructed molecules provided an excellent agreement. Furthermore, the viscosity for the hemicellulose and lignin molecules was found to be 39 and 19 Pa·s, 28 and 15 Pa·s, respectively, which was at a magnitude close to the viscosity of 3 Pa·s, demonstrated for the collagen molecule using MD simulation (Gautieri et al., 2012). The relatively higher viscosity in the case of hemicellulose and lignin molecules, compared to a collagen molecule, could be attributed to the larger number of non-bonded segments: under constant force creep, the segments in the hemicellulose and lignin molecule could slide more freely, and the breakage and reforming of non-bonded interactions could be more frequent; thus, their viscous behavior could be more pronounced than that in the collagen molecule with a triple helical configuration.

Based on the calculated elastic modulus and viscosity, it could be indicated that even if the constructed molecules are simplified models from the realistic structures, they seem representative enough to allow us to draw general conclusions on the viscoelastic properties of bamboo at the molecular level. Specifically, the elastic response of bulk bamboo could be mainly attributed to the elastic deformation in the backbone of crystalline cellulose, the amorphous hemicellulose and lignin matrix, whereas the viscous behavior could be largely corresponded to the viscous properties of the hemicellulose and lignin matrix. It is worth mentioning that, in natural materials, cellulose molecules could be partially arranged in a strongly disordered manner, so called paracrystalline or amorphous cellulose (Wang et al., 2012), which could reduce the E of

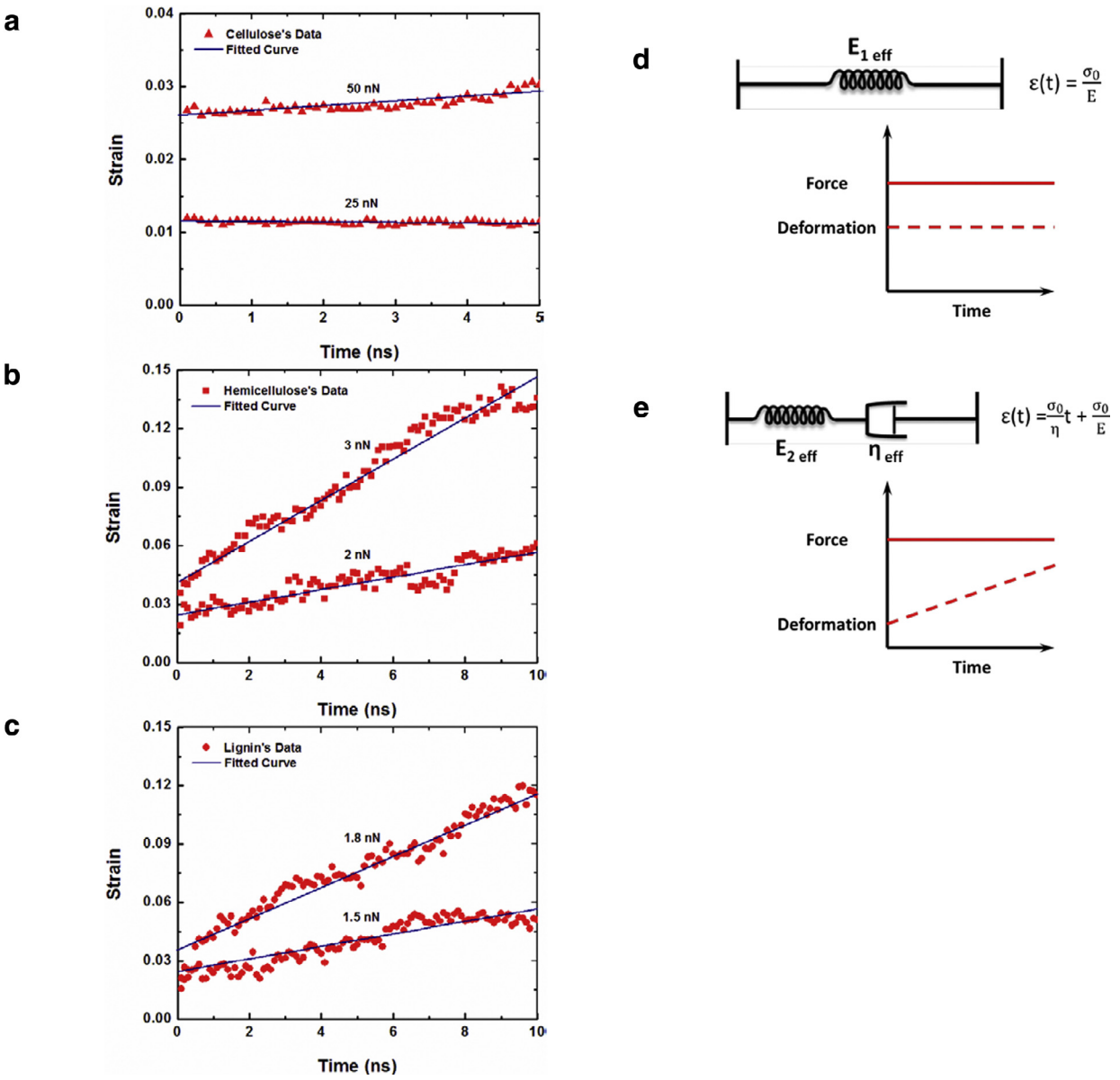

Fig. 9. Single molecule creep test: Mechanical responses to the molecule creep tests of (a) crystalline cellulose, (b) amorphous hemicellulose and (c) amorphous lignin. Dots represent the simulation data, whereas lines represent the fitted curves using a Hookean spring model for (d) crystalline cellulose and a Maxwellian model for (e) amorphous hemicellulose and amorphous lignin molecules, respectively.

cellulose microfibrils at a magnitude of 10 GPa (Lejeune and Deprez, 2010). In addition, the cellulose at paracrystalline or amorphous state might behave as viscoelastic materials, and contribute to the viscoelastic behaviors observed at larger scales. Future work could look further and study the viscoelastic properties of paracrystalline and amorphous cellulose.

3.6. Underlying mechanisms for microstructural viscoelasticity

To contribute to the exhibited macroscopic viscoelastic behavior in bulk bamboo, it is disclosed that the microstructural constituents of bamboo have behaved distinctly different in the course of the dynamic loading. The disclosed different behavior of fibers and parenchyma cells, when subjected to similar dynamic nano-indentation loading, is basically attributed to their different microstructures. It is disclosed that, both parenchyma cells and fibers are mainly constituted by cellulose microfibrils embedded in a lignin and hemicellulose matrix, whereas the orientation of microfibrils alongside the amount and the extent of lignin and lignification (lignification refers to a complex process which involves the disposition of lignin on the extracellular polysaccharide matrix), respectively, is different in the case of both (Wang et al., 2011). Compared

to parenchyma cells, fibers possess and exhibit smaller amount but higher extent of lignin and lignification, respectively: our MD simulations demonstrated that the hemicellulose and lignin are largely responsible for the viscoelastic behavior of bamboo at the molecular level and accordingly the difference in the lignin amongst the fibers and parenchyma cells could result in their viscosity variation. The observation of viscosity variation with duration of applied stress (see Fig. 8c–d) also revealed that the structure of both fibers and parenchyma cells depends on the duration of the applied stress: although the fibers and parenchyma cells have similar multi-layered cell wall structure, the fibers have a thicker cell wall. Accordingly, when the fiber is sheared, a more open space would be generated in the cell wall structure, which could allow a more pronounced disordering process, which result in the disclosed decline in viscosity with stress duration, a representative of shear thinning behavior. On the contrary, the demonstrated rise in the viscosity with stress duration, in the case of parenchyma cells, is a character of shear thickening behavior which usually results from a certain kind of stress-induced ordering process. In such a case, the molecules in the thin cell wall could be lined up, along the shearing direction, which could lead to the increase in the local density along with the viscosity.

Pertaining to the demonstrated variations in viscosity of fibers and parenchyma cells with respect to duration of applied stress, it is concluded that both fibers and parenchyma cells contribute in determining the overall viscoelastic damping behavior in bulk bamboo structure. In view of the nature of the loadings in the case of both macroscopic and microscopic cases, it is reasonable to presume that the duration of the applied stress in low loading frequencies ($f \leq 1.0$ Hz), in the case of bulk bamboo, is almost similar to the $t_h \geq 1$ s, in the case of nano-indentation experiments on bamboo's microstructural constituents. Similarly, it is sensible to consider that the duration of the loading in the case of $f > 1.0$ Hz, in the case of macroscopic loading, is almost similar to the $t_h < 1$ s in the case of nano-indentation experiments. So, in view of the relatively small and large recorded viscosities for fibers and parenchyma cells, respectively, in the case of large duration of applied stress ($t_h \geq 1$ s) (see Fig. 8c–d), it is reasonable to speculate that in the case of low loading frequencies ($f \leq 1.0$ Hz), fibers behave almost as an elastic phase, whereas the very small viscoelasticity in bulk structure of bamboo is stemmed out from the contribution of parenchyma cells. However, as the duration of loading reduced, the contribution of fibers in viscoelasticity of bulk bamboo increased and both fibers and parenchyma cells played almost equally to create the overall viscoelasticity of bulk bamboo. As depicted in Fig. 8c–d, both fibers and parenchyma cells demonstrated almost similar viscosity in the case of very fast loading/unloading, given that fibers and parenchyma cells, respectively, exhibited a viscosity of~2.0–3.6 GPa.s and ~1.8–3.0 GPa.s.

3.7. Role of moisture content on bamboo's viscoelastic behaviors

The molecular models in the present study include only the three main constituents of bamboo microstructure, including cellulose, hemicellulose and lignin. Moisture content in bamboo, which can also regulate the material's properties, is not considered here, as most structural applications use processed, desiccated bamboo materials. However, our previous study on the chitin–protein composite shows the importance of equilibrium moisture content on the material's properties (Yu and Lau, 2015): chitin–protein composite is the structural material of many marine animals including lobster, squid, and sponge, and it is found that the dehydrated chitin–protein composite exhibits higher elastic modulus compared to that in the hydrated state. It is thus expected that the equilibrium moisture content in bamboo may affect its viscoelastic behavior as well, and a systematic follow-up study is required to find out the quantitative variations of viscoelastic behaviors at different hierarchical scales of structural bamboo materials in the presence of moisture.

4. Conclusions

The intrinsic viscoelastic mechanical behavior of structural bamboo material has been systematically studied here at multiscale, to understand the viscoelasticity in hierarchical biological structures from the macroscopic scale down to the molecular scale. It has been demonstrated that desiccated bamboo culm exhibited a viscoelastic damping behavior, when subjected to dynamic compressive loading, given that the viscosity (η) and the volume fraction of viscous phases (χ) significantly increased with increase in loading frequency. At low loading frequencies, the small evolved viscous phases within the parenchyma cells were mainly responsible for the small viscoelasticity in bulk bamboo, whereas the disclosed large viscoelasticity in bulk bamboo under high loading frequencies was stemmed out from the concurrent contribution of fibers and the parenchyma cells. Furthermore, it has been disclosed that the hemicellulose and lignin matrix largely contribute to the microscale viscoelastic behavior of bamboo's microstructural constituents as well as the macroscopic viscoelastic behavior observed in bulk bamboo structures. It is expected that the present study, including multi-scale mechanical experiments coupled with computational approaches, could provide valuable insights for designing bamboo-inspired composites with desired damping behavior as well as understanding the intrinsic viscoelasticity in other hierarchical-structured biological materials. Moreover, the obtained simulation results will be very important input for developing the mesoscale model of fibers and parenchyma cells by using the coarse-grained technique, which is of great use to characterize the viscoelastic behavior of bamboo's microstructural constituents from the bottom–up approach.

Acknowledgments

The authors gratefully thank Dr. Amit Banerjee for the valuable discussions on the numerical modeling. The authors also thank Mr. Arash Samaei, Dr. Jifang Zeng, Prof. Yong Yang and Prof. Xinrui Niu at City University of Hong Kong for the help on the nanomechanical testing and the nano-indentation analysis. M.K. Habibi acknowledges the support from CityU International Transition Team scheme (ITT-GTA) Postdoctoral Fellowship. This work was supported by City University of Hong Kong under the ARG grants # 9667098 and # 9667117.

The authors have no competing interests in this work.

Supplementary Materials

Supplementary material associated with this article can be found, in the online version, at doi:10.1016/j.mechmat.2016.03.002.

References

Scurlock, J., Dayton, D., Hames, B., 2000. Bamboo: an overlooked biomass resource? Biomass and Bioenergy 19, 229–244.
Chung, K.F., Yu, W.K., 2002. Mechanical properties of structural bamboo for bamboo scaffoldings. Eng. Struct. 24, 429–442.
Gibson, L.J., 2012. The hierarchical structure and mechanics of plant materials. J. Royal Soc. Interface 9, 2749–2766.
Dixon, P.G., Gibson, L.J., 2014. The structure and mechanics of Moso bamboo material. J. Royal Soc. Interface 11, 20140321.
Silva, E.C.N., Walters, M.C., Paulino, G.H., 2006. Modeling bamboo as a functionally graded material: lessons for the analysis of affordable materials. J. Mater. Sci. 41, 6991–7004.
Wegst, U.G.K., Bai, H., Saiz, E., Tomsia, A.P., Ritchie, R.O., 2015. Bioinspired structural materials. Nat. Mater. 14, 23–36.
Habibi, M.K., Samaei, A.T., Gheshlaghi, B., Lu, J., Lu, Y., 2015. Asymmetric flexural behavior from bamboo's functionally graded hierarchical structure: underlying mechanisms. Acta Biomater. 16, 178–186.
Habibi, M.K., Lu, Y., 2014. Crack propagation in bamboo's hierarchical cellular structure. Sci. Rep. 4:05598.
Huang D., Zhou A., Li H., Su Y., Chen G., 2012. Experimental study on the tensile properties of bamboo related to its distribution of vascular bundles. Key Engineering Materials 517, 112-117.
Low, I.M., Che, Z.Y., Latella, B.A., 2006. Mapping the structure, composition and mechanical properties of bamboo. J. Mater. Res. 21, 1969–1976.
Obataya, E., Kitin, P., Yamauchi, H., 2007. Bending characteristics of bamboo (Phyllostachys pubescens) with respect to its fiber-foam composite structure. Wood Sci. Technol. 41, 385–400.
Shao, Z.-P., Fang, C.-H., Tian, G.-L., 2009. Mode I interlaminar fracture property of moso bamboo (Phyllostachys pubescens). Wood Sci. Technol. 43, 527–536.
Tan, T., Rahbar, N., Allameh, S.M., Kwofie, S., Dissmore, D., Ghavami, K., et al., 2011. Mechanical properties of functionally graded hierarchical bamboo structures. Acta Biomater. 7, 3796–3803.
Wegst, U.G.K., 2008. Bamboo and wood in musical instruments. Mater. Res. 38, 323.
Jain, S., Kumar, R., Jindal, U.C., 1992. Mechanical behaviour of bamboo and bamboo composite. J. Mater. Sci. 27, 4598–4604.
Li, M.-F., Fan, Y.-M., Xu, F., Sun, R.-C., Zhang, X.-L., 2010. Cold sodium hydroxide/urea based pretreatment of bamboo for bioethanol production: characterization of the cellulose rich fraction. Ind. Crops Prod. 32, 551–559.
Li, M.-F., Fan, Y.-M., Xu, F., Sun, R.-C., 2011. Structure and thermal stability of polysaccharide fractions extracted from the ultrasonic irradiated and cold alkali pretreated bamboo. J. Appl. Polym. Sci. 121, 176–185.
Li, M.-F., Shen, Y., Sun, J.-K., Bian, J., Chen, C.-Z., Sun, R.-C., 2015. Wet torrefaction of bamboo in hydrochloric acid solution by microwave heating. ACS Sustainable Chem. Eng. 3, 2022–2029.
Yamashita, J., Furman, B.R., Rawls, H.R., Wang, X., Agrawal, C.M., 2001. The use of dynamic mechanical analysis to assess the viscoelastic properties of human cortical bone. J. Biomed. Mater. Res. 58, 47–53.
Sewda, K., Maiti, S.N., 2013. Dynamic mechanical properties of high density polyethylene and teak wood flour composites. Polym. Bull. 70, 2657–2674.
Jiang, J., Lu, J., Zhao, Y., Wu, Y., 2010. Influence of frequency on wood viscoelasticity under two types of heating conditions. Drying Technol. 28, 823–829.
Zhang, T., Bai, S.L., Zhang, Y.F., Thibaut, B., 2012. Viscoelastic properties of wood materials characterized by nanoindentation experiments. Wood Sci. Technol. 46, 1003–1016.
Shepherd, T.N., Zhang, J., Ovaert, T.C., Roeder, R.K., Niebur, G.L., 2011. Direct comparison of nanoindentation and macroscopic measurements of bone viscoelasticity. J. Mech. Behav. Biomed. Mater. 4, 2055–2062.
Amada, S., Lakes, R., 1997. Viscoelastic properties of bamboo. J. Mater. Sci. 32, 2693–2697.
Yu, Y., Jiang, Z.H., Fei, B.H., Wang, G., Wang, H.K., 2011. An improved microtensile technique for mechanical characterization of short plant fibers: a case study on bamboo fibers. J. Mater. Sci. 46, 739–746.
Sun, Y., Lin, L., Deng, H., Li, J., He, B., Sun, R., et al., 2008. Structural changes of bamboo cellulose in formic acid. BioResour. 3, 297–315.
Gomes, T.C., Skaf, M.S., 2012. Cellulose-builder: a toolkit for building crystalline structures of cellulose. J. Comput. Chem. 33, 1338–1346.
Wang, Y., Leppänen, K., Andersson, S., Serimaa, R., Ren, H., Fei, B., 2012. Studies on the nanostructure of the cell wall of bamboo using X-ray scattering. Wood Sci. Technol. 46, 317–332.
Maekawa, E., 1976. Studies on hemicellulose of bamboo. Wood Res. Bull. Wood Res. Inst. Kyoto Univ. 59, 153–179.
Charlier, L., Mazeau, K., 2012. Molecular modeling of the structural and dynamical properties of secondary plant cell walls: Influence of lignin chemistry. J. Phys. Chem. B 116, 4163–4174.
Jin, K., Qin, Z., Buehler, M.J., 2015. Molecular deformation mechanisms of the wood cell wall material. J. Mech. Behav. Biomed. Mater. 42, 198–206.
Wen, J.-L., Sun, S.-L., Xue, B.-L., Sun, R.-C., 2013. Quantitative structural characterization of the lignins from the stem and pith of bamboo (Phyllostachys pubescens). Holzforschung 67, 613–627.
Tam, L-h., Lau, D., 2014. A molecular dynamics investigation on the cross-linking and physical properties of epoxy-based materials. RSC Adv. 4, 33074–33081.
Plimpton, S., 1995. Fast parallel algorithms for short-range molecular dynamics. J. Comput. Phys. 117, 1–19.
Sun, H., Mumby, S.J., Maple, J.R., Hagler, A.T., 1994. An ab initio CFF93 all-atom force field for polycarbonates. J. Am. Chem. Soc. 116, 2978–2987.
Sun, H., 1995. Ab initio calculations and force field development for computer simulation of polysilanes. Macromolecules 28, 701–712.
Mazeau, K., Heux, L., 2003. Molecular dynamics simulations of bulk native crystalline and amorphous structures of cellulose. J. Phys. Chem. B 107, 2394–2403.
Tanaka, F., Iwata, T., 2006. Estimation of the elastic modulus of cellulose crystal by molecular mechanics simulation. Cellulose 13, 509–517.
Hanus, J., Mazeau, K., 2006. The xyloglucan–cellulose assembly at the atomic scale. Biopolymers 82, 59–73.
Da Silva Perez, D., Ruggiero, R., Morais, L.C., Machado, A.E.H., Mazeau, K., 2004. Theoretical and experimental studies on the adsorption of aromatic compounds onto cellulose. Langmuir 20, 3151–3158.
Rahman, R., Foster, J., Haque, A., 2013. Molecular dynamics simulation and characterization of graphene–cellulose nanocomposites. J. Phys. Chem. A 117, 5344–5353.
Cifre, J.G.H., Hess, S., Kröger, M., 2004. Linear viscoelastic behavior of unentangled polymer melts via non-equilibrium molecular dynamics. Macromol. Theory Simulat. 13, 748–753.
Simoes, R., Cunha, A.M., Brostow, W., 2006. Molecular dynamics simulations of polymer viscoelasticity: effect of the loading conditions and creep behaviour. Model. Simulat. Mater. Sci. Eng. 14, 157.
Gautieri, A., Vesentini, S., Redaelli, A., Buehler, M.J., 2012. Viscoelastic properties of model segments of collagen molecules. Matrix Biol. 31, 141–149.
Youssefian, S., Rahbar, N., 2015. Molecular origin of strength and stiffness in bamboo fibrils. Sci. Rep. 5:11116.
Poletto, M., Zeni, M., Zattera, A.J., 2012. Dynamic mechanical analysis of recycled polystyrene composites reinforced with wood flour. J. Appl. Polym. Sci. 125, 935–942.
Huo, L., Ma, J., Ke, H., Bai, H., Zhao, D., Wang, W., 2012. The deformation units in metallic glasses revealed by stress-induced localized glass transition. J. Appl. Phys. 111, 113522.
Huo, L., Zeng, J., Wang, W., Liu, C.T., Yang, Y., 2013. The dependence of shear modulus on dynamic relaxation and evolution of local structural heterogeneity in a metallic glass. Acta Mater. 61, 4329–4338.

Ngan, A., Tang, B., 2002. Viscoelastic effects during unloading in depth-sensing indentation. J. Mater. Res. 17, 2604–2610.
Feng, G., Ngan, A., 2002. Effects of creep and thermal drift on modulus measurement using depth-sensing indentation. J. Mater. Res. 17, 660–668.
Lejeune, A., Deprez, T., 2010. Cellulose: Structure and Properties, Derivatives and Industrial Uses. Nova Science Publishers, Incorporated.
Wang, X., Ren, H., Zhang, B., Fei, B., Burgert, I., 2011. Cell wall structure and formation of maturing fibres of moso bamboo (Phyllostachys pubescens) increase buckling resistance. J. Royal Soc. Interface 9, 988–996.
Yu, Z., Lau, D., 2015. Molecular dynamics study on stiffness and ductility in chitin–protein composite. J. Mater. Sci. 50, 7149–7157.